

This discussion paper is/has been under review for the journal Atmospheric Chemistry and Physics (ACP). Please refer to the corresponding final paper in ACP if available.

Development of an atmospheric N₂O isotopocule model and optimization procedure, and application to source estimation

K. Ishijima¹, M. Takigawa¹, K. Sudo^{2,1}, S. Toyoda³, N. Yoshida^{4,5}, T. Röckmann⁶, J. Kaiser⁷, S. Aoki⁸, S. Morimoto⁸, S. Sugawara⁹, and T. Nakazawa⁸

¹Department of Environmental Geochemical Cycle Research, JAMSTEC, Yokohama, Japan

²Graduate School of Environmental Studies, Nagoya University, Nagoya, Japan

³Department of Environmental Science and Technology, Tokyo Institute of Technology, Yokohama, Japan

⁴Department of Environmental Chemistry and Engineering, Tokyo Institute of Technology, Yokohama, Japan

⁵Earth-Life Science Institute, Tokyo Institute of Technology, Tokyo, Japan

⁶Institute for Marine and Atmospheric research Utrecht, Utrecht University, Utrecht, the Netherlands

⁷Centre for Ocean and Atmospheric Sciences, School of Environmental Sciences, University of East Anglia, Norwich, UK

19947

⁸Center for Atmospheric and Oceanic Studies, Tohoku University, Sendai, Japan

⁹Miyagi University of Education, Sendai, Japan

Received: 31 May 2015 – Accepted: 29 June 2015 – Published: 22 July 2015

Correspondence to: K. Ishijima (ishijima@jamstec.go.jp)

Published by Copernicus Publications on behalf of the European Geosciences Union.

19948

Discussion Paper

Discussion Paper

Discussion Paper

Discussion Paper

Discussion Paper

Discussion Paper

Discussion Paper

Discussion Paper

Abstract

This paper presents the development of an atmospheric N₂O isotopocule model based on a chemistry-coupled atmospheric general circulation model (ACTM). We also describe a simple method to optimize the model and present its use in estimating the isotopic signatures of surface sources at the hemispheric scale. Data obtained from ground-based observations, measurements of firn air, and balloon and aircraft flights were used to optimize the long-term trends, interhemispheric gradients, and photolytic fractionation, respectively, in the model. This optimization successfully reproduced realistic spatial and temporal variations of atmospheric N₂O isotopocules throughout the atmosphere from the surface to the stratosphere. The very small gradients associated with vertical profiles through the troposphere and the latitudinal and vertical distributions within each hemisphere were also reasonably simulated. The results of the isotopic characterization of the global total sources were generally consistent with previous one-box model estimates, indicating that the observed atmospheric trend is the dominant factor controlling the source isotopic signature. However, hemispheric estimates were different from those generated by a previous two-box model study, mainly due to the model accounting for the interhemispheric transport and latitudinal and vertical distributions of tropospheric N₂O isotopocules. Comparisons of time series of atmospheric N₂O isotopocule ratios between our model and observational data from several laboratories revealed the need for a more systematic and elaborate intercalibration of the standard scales used in N₂O isotopic measurements in order to capture a more complete and precise picture of the temporal and spatial variations in atmospheric N₂O isotopocule ratios. This study highlights the possibility that inverse estimation of surface N₂O fluxes, including the isotopic information as additional constraints, could be realized.

19949

1 Introduction

Nitrous oxide (N₂O) is currently one of the most remarkable atmospheric components of the Earth's environment, being both a greenhouse gas with high radiative efficiency (100 year global warming potential or global temperature change potential of 200–300; Ciais et al., 2013), as well as the most influential ozone depleting substance (ODS) emitted during this century, when CFC emissions have been largely reduced following the Montreal Protocol (Ravishankara et al., 2009). N₂O was originally a natural gas component that was shown (from ice core records) to have existed prehistorically in the atmosphere (Schilt et al., 2010), and was mainly produced as an intermediate product or by-product during microbial utilization of nitrogen compounds in soils or oceans. Generated in this way on the Earth's surface, N₂O is chemically inert in the troposphere. However, in the stratosphere, N₂O is decomposed by photolysis and reaction with O(¹D). The latter reaction is a source of nitric oxide (NO), which is a main player for stratospheric ozone depletion.

Around the mid-19th century, as industrialization expanded, the atmospheric N₂O mole fraction began to increase, and this growth was further accelerated in the 20th century (Machida et al., 1995; MacFarling Meure et al., 2006) following the increase in global population. This increase in N₂O levels is thought to have been caused by the use of synthetic nitrogen fertilizers developed during the industrialization of the agricultural sector. Through the application of nitrogen fertilizers onto crops, the amount of nitrogen compounds available for microbes increased, and N₂O production inevitably increased in the soil. It would be difficult to quickly reduce nitrogen fertilizer use in crop production (in order to reduce N₂O emissions) if we continue to feed the rapidly increasing global population. Thus, the increase in the atmospheric N₂O mole fraction has continued at a rate of around 0.5–0.8 nmol mol⁻¹ a⁻¹ near the surface since the 1980s (Ciais et al., 2013). Various N₂O sources other than agricultural soils are known, and the sum of their emissions (2.8 Tg a⁻¹ N equivalents) is considered to be about 30 % less than agricultural soil emissions alone (4.1 Tg a⁻¹ N), but the contri-

19950

5 bution from each source to the global total is still only poorly understood and there are large uncertainties in the estimates (Ciais et al., 2013). Emission estimates for individual source categories are mainly derived from bottom-up approaches that combine field flux measurements and statistical data (e.g., data on nitrogen fertilizer use in a given region), but large spatiotemporal variations in the N₂O flux exist at the site to local scales. Consequently, it is difficult to make representative and accurate emission estimates for each source, and thus develop strategies to efficiently reduce N₂O emissions at global and national levels.

10 One approach to separating out the contributions from individual sources is the use of isotopically-substituted molecules, or, short, isotopocules (Kaiser and Röckmann, 2008). The isotopocule ratio of N₂O is altered by various biogeochemical processes, such as biogenic production and consumption in the source areas, and also by chemical processes in the atmosphere. The isotopic composition of the precursors is also reflected to some degree in the resultant N₂O. Therefore, it is thought that stable isotopocule ratios could be used to quantify the contribution from individual N₂O sources. There have been many studies of the isotopic signatures of various N₂O sources and sinks, but a unique isotopic value for each source with an adequately small uncertainty range remains elusive because of the complicated tangle of the precursor's isotopic signatures and microbial process-driven isotopic fractionation (e.g., Kim and Craig, 1993; Rahn and Wahlen, 2000; Toyoda et al., 2011, 2015). There have also been experimental or theoretical studies of isotopic fractionation driven by photochemical loss reactions (e.g., Selwyn and Johnston, 1981; Kaiser et al., 2002, 2003a; Nanbu and Johnson, 2004; von Hessberg et al., 2004; Schmidt et al., 2011). This fractionation generates large vertical gradients in N₂O mole fraction and isotopocule ratios, which decrease and increase, respectively, with increasing altitude in the stratosphere (e.g., Kim and Craig, 1993; Park et al., 2004; Toyoda et al., 2004; Kaiser et al., 2006). For the troposphere, and based on ice core analysis, firn air analysis, or direct atmospheric measurements, long-term trends have been mainly studied for the period from the mid-1700s to the present (Sowers et al., 2002; Röckmann et al., 2003; Röckmann and

19951

Levin, 2005; Bernard et al., 2006; Ishijima et al., 2007), although some recent studies have discussed seasonal cycles or interhemispheric differences (Park et al., 2012; Toyoda et al., 2013). These studies have revealed that the observed decreasing trends of, for example, the major nitrogen and oxygen isotope ratios of N₂O, are caused by the continuous input of N₂O into the troposphere from anthropogenic sources, which, based on a top-down approach using a simple box model and observed data, are estimated to be on average isotopically lighter than tropospheric N₂O (Toyoda et al., 2015).

15 It is now necessary to progress to the next stage of integrating the knowledge obtained (as above), and to comprehensively validate this knowledge, in order to reconsider how and what should be the focus of study in this field. Global three-dimensional (3-D) modelling is considered a possible avenue for such research. There have already been some attempts at global N₂O isotopocule modelling (McLinden et al., 2003; Morgan et al., 2004; Liang and Yung, 2007), but existing models have a fixed N₂O mole fraction in the lower troposphere and no surface emissions, or are sometimes two-dimensional, and this is because they were developed mainly to examine photochemistry-induced isotopocule fractionation in the stratosphere. On the other hand, several studies have performed global N₂O inverse modelling to estimate regional fluxes (Hirsch et al., 2006; Huang et al., 2008; Thompson et al., 2014a; Saikawa et al., 2014). The derived regional N₂O emission estimates are generally reasonable, predominantly because of recently improved observation networks incorporating flask sampling and in situ measurements (e.g., Dlugokencky et al., 1994; Tohjima et al., 2000; Prinn et al., 2000; Ishijima et al., 2009). However, it is still thought that some of the uncertainty in inverse estimations is caused by poor simulation of the stratosphere–troposphere exchange (STE), which brings stratospheric N₂O-depleted air into the troposphere and influences spatiotemporal variations in the tropospheric mole fraction. In terms of isotopocules, the N₂O thus introduced into the troposphere by STE is rich in heavier isotopocules, as N₂O is enriched in heavier isotopocules in the stratosphere by photochemical loss processes; therefore, as discussed by Park et al. (2012), isotopocules can be used to estimate the effect of STE on tropospheric N₂O mole frac-

19952

tions. Unfortunately, atmospheric N₂O isotopocule measurements have not reached the level required for such inverse modelling or STE studies in terms of measurement precision and number of stations. However, in the near future, when high-frequency and high-precision optical measurement systems capable of continuously monitoring atmospheric N₂O isotopocule ratios (e.g., Waechter et al., 2008) are improved and become more widely available, global atmospheric N₂O isotopocule models could be essential to our understanding of observed results (e.g., see Rigby et al., 2012 for the case of methane). Therefore, in this study we present an outline of a newly developed N₂O isotopocule model that explicitly handles surface emissions, together with a simple approach to optimizing the model's photochemical fractionation and surface emissions using several types of observational data.

2 N₂O isotopocules

2.1 Notation for N₂O isotopocules

In this study, we use the term “isotopocule”, which was first proposed by Kaiser and Röckmann (2008) and has also recently been adopted by Coplen (2011) to designate isotopically substituted molecules. The term encompasses the terms “isotopologue” (a molecule differing only in isotopic composition; e.g., ¹⁴N¹⁴N¹⁶O and ¹⁴N¹⁴N¹⁸O) and “isotopomer” (molecules having the same number of each isotopic atom but differing in their positions; e.g., ¹⁴N¹⁵N¹⁶O and ¹⁵N¹⁴N¹⁶O). Individual N₂O isotopocules are distinguished by their molecular formula. We consider the following four N₂O isotopocules: ¹⁴N¹⁴N¹⁶O, ¹⁴N¹⁵N¹⁶O, ¹⁵N¹⁴N¹⁶O, and ¹⁴N¹⁴N¹⁸O in this study, and the notation of the isotopocule ratios is as follows (Toyoda and Yoshida, 1999):

19953

$$\delta^{15}\text{N}^i = {}^{15}\text{R}_{\text{sample}}^i / {}^{15}\text{R}_{\text{std}}^i - 1, \quad (i = \text{bulk}, \alpha \text{ or } \beta) \quad (1)$$

$$\delta^{18}\text{O} = {}^{18}\text{R}_{\text{sample}} / {}^{18}\text{R}_{\text{std}} - 1, \quad (2)$$

$${}^{15}\text{R}^\alpha = [{}^{14}\text{N}^{15}\text{N}^{16}\text{O}] / [{}^{14}\text{N}^{14}\text{N}^{16}\text{O}], \quad (3)$$

$${}^{15}\text{R}^\beta = [{}^{15}\text{N}^{14}\text{N}^{16}\text{O}] / [{}^{14}\text{N}^{14}\text{N}^{16}\text{O}], \quad (4)$$

$${}^{15}\text{R}^{\text{bulk}} = ({}^{15}\text{R}^\alpha + {}^{15}\text{R}^\beta) / 2, \quad (5)$$

$${}^{18}\text{R} = [{}^{14}\text{N}^{14}\text{N}^{18}\text{O}] / [{}^{14}\text{N}^{14}\text{N}^{16}\text{O}]. \quad (6)$$

We also use the ¹⁵N site preference (hereafter $\delta^{15}\text{N}^{\text{sp}}$), which is defined as the difference between the two nitrogen isotopomer deltas:

$$\delta^{15}\text{N}^{\text{sp}} = \delta^{15}\text{N}^\alpha - \delta^{15}\text{N}^\beta. \quad (7)$$

We note that in some publications, a different notation for the N₂O isotopomers was used, following Brenninkmeijer and Röckmann (1999). In publications from this group, $\delta^{15}\text{N}^\alpha$ is denoted ${}^2\delta^{15}\text{N}$ and $\delta^{15}\text{N}^\beta$ is denoted ${}^1\delta^{15}\text{N}$. Hereafter, we use “isotopocule deltas” as an inclusive term for $\delta^{15}\text{N}^{\text{bulk}}$, $\delta^{18}\text{O}$, $\delta^{15}\text{N}^\alpha$, $\delta^{15}\text{N}^\beta$, and $\delta^{15}\text{N}^{\text{sp}}$.

2.2 Conversion of isotopocule ratio to mole fraction

When we simulate N₂O isotopocules in a model or use the observational data to optimize the model, the isotopocule ratios must be converted to the absolute mole fractions. In this study, we calculated each isotopocule mole fraction assuming that N₂O consists of only four isotopocules: ¹⁴N¹⁴N¹⁶O, ¹⁴N¹⁵N¹⁶O, ¹⁵N¹⁴N¹⁶O, and ¹⁴N¹⁴N¹⁸O as follows:

$$[\text{N}_2\text{O}] = [{}^{14}\text{N}^{14}\text{N}^{16}\text{O}] + [{}^{14}\text{N}^{15}\text{N}^{16}\text{O}] + [{}^{15}\text{N}^{14}\text{N}^{16}\text{O}] + [{}^{14}\text{N}^{14}\text{N}^{18}\text{O}]. \quad (8)$$

By substituting Eqs. (3), (4), and (6) into Eq. (8), we have

$$[{}^{14}\text{N}^{14}\text{N}^{16}\text{O}] = [\text{N}_2\text{O}] / (1 + {}^{15}\text{R}^\alpha + {}^{15}\text{R}^\beta + {}^{18}\text{R}). \quad (9)$$

19954

As these four isotopocules account for more than 99.9% of all of the atmospheric N₂O isotopocules, and assuming statistical isotope distributions for the three atoms in the N₂O molecule ($x(^{14}\text{N}^{14}\text{N}^{16}\text{O}) = 99.01\%$, $x(^{14}\text{N}^{15}\text{N}^{16}\text{O}) = 0.37\%$, $x(^{15}\text{N}^{14}\text{N}^{16}\text{O}) = 0.36\%$, and $x(^{14}\text{N}^{14}\text{N}^{18}\text{O}) = 0.21\%$), neglecting less abundant species, will not generate any significant errors in the N₂O isotopocule ratios finally obtained.

3 Observational data

We used three sets of observation data in the model optimization and analysis in this study. Table 1 and Fig. 1 summarize the details of the ground-based stations and the locations of all observations, respectively.

10 3.1 Time series data observed at a ground-based station

We used the high-precision N₂O isotopocule ratio measurements of Röckmann and Levin (2005). Air sampling was performed at the German Antarctic research station Neumayer (71° S, 8° W, hereafter NMY) by the Alfred Wegener Institute for Polar Research (AWI, Bremerhaven) since the early 1980s. From this dataset, twenty-three
 15 archived air samples for the period from March 1990 to November 2002 were analysed for N₂O mole fraction at the University of Heidelberg (Schmidt et al., 2001) using ECD-GC (an Electron Capture Detector equipped Gas Chromatography), based on a standard scale developed by The Advanced Global Atmospheric Gases Experiment (AGAGE), and also a high-precision isotopocule ratio measurement technique
 20 (Röckmann et al., 2005) for isotopocule ratios at the Max Planck Institute for Nuclear Physics (Heidelberg). This dataset shows highly stable temporal variations (standard error about 0.14 nmol mol⁻¹, 0.01, 0.02, 0.07, and 0.06‰ for the mole fraction, $\delta^{15}\text{N}^{\text{bulk}}$, $\delta^{18}\text{O}$, $\delta^{15}\text{N}^{\alpha}$, and $\delta^{15}\text{N}^{\beta}$, respectively) compared with other datasets (Park et al., 2012; Toyoda et al., 2013), because the measurement precision was very high,
 25 and also the station is very close to being a true background site and so is less af-

19955

ected by nearby sources. The advantage is obvious in comparison with other stations showing highly variable results and sometimes blurring the trends due to low measurement precisions and/or local source influences (Fig. 10). Consequently, this dataset was considered suitable for the first step of developing an N₂O isotopocule model with
 5 simplified surface emissions of a spatiotemporally constant isotopocule ratio. In Röckmann and Levin (2005), results for $\delta^{15}\text{N}^{\alpha}$ and $\delta^{15}\text{N}^{\beta}$ are shown using two different standard scales from the Max-Planck Institute (Kaiser et al., 2003b) and the Tokyo Institute of Technology (Toyoda and Yoshida, 1999), but we used the latter scale, which has been supported by further reports (Griffith et al., 2009; Westley et al., 2007), for all
 10 data in this study.

3.2 Time series data reconstructed from analysis of firn air obtained from the polar ice sheets

We also used historical data of atmospheric N₂O mole fraction and isotopocule ratios, which were reconstructed from analysis of firn air samples obtained from three stations in both the Arctic and Antarctic regions (Ishijima et al., 2007; Table 1; Fig. 1);
 15 North GRIP (75° N, 43° W, 2959 m a.s.l., hereafter NGR), Greenland, Dome Fuji (77° S, 40° E, 3810 m a.s.l., hereafter DFJ) and H72 (69° S, 41° E, 1241 m a.s.l.), Antarctica. Measurement precision (N₂O: 0.3 nmol mol⁻¹; $\delta^{15}\text{N}^{\text{bulk}}$: 0.1‰; $\delta^{18}\text{O}$: 0.2‰) was not as high as the data from NMY, but only the decadal means of the record, which improves the standard error of the data, were used to limit the uncertainty in this study.
 20 The standard scale was not adjusted to derive the interhemispheric differences, because all firn air samples were measured using a single analytical system with the same standard scale. Thus, we can ignore uncertainties caused by the standard scale difference, and it is a great advantage of this dataset.

19956

oda et al. (2004), and then interpolated the constants for $^{14}\text{N}^{15}\text{N}^{16}\text{O}$ and $^{15}\text{N}^{14}\text{N}^{16}\text{O}$ to obtain that of $^{14}\text{N}^{14}\text{N}^{18}\text{O}$ so that the relationship of the εs of $\delta^{15}\text{N}^\alpha$, $\delta^{15}\text{N}^\beta$, and $\delta^{18}\text{O}$ was the same as that of the fractionation constants of $^{14}\text{N}^{15}\text{N}^{16}\text{O}$, $^{15}\text{N}^{14}\text{N}^{16}\text{O}$, and $^{14}\text{N}^{14}\text{N}^{18}\text{O}$. However, these photolytic fractionations implemented in the model were found to underestimate the observed εs , so we slightly modified the fractionation in the model using a simple optimization method, as described in Sect. 4.2.3. For oxidation with $\text{O}(^1\text{D})$, we used the mean fractionation constants determined by Kaiser et al. (2002), but we did not consider temperature dependence of the fractionations, which are very small and thus do not contribute strongly to the fractionations in the stratosphere compared to the photolytic fractionations. The four different species, $^{14}\text{N}^{14}\text{N}^{16}\text{O}$, $^{14}\text{N}^{15}\text{N}^{16}\text{O}$, $^{15}\text{N}^{14}\text{N}^{16}\text{O}$, and $^{14}\text{N}^{14}\text{N}^{18}\text{O}$, are calculated separately in the model.

4.1.3 Emission scenarios

We included the four source categories of N_2O emissions in the model simulations in this study; i.e., natural soils, oceans, anthropogenic, and biomass burning emissions. The annual mean natural soil emissions of N_2O were taken from the Emission Database for Global Atmospheric Research version 2 (EDGARv2; http://themasites.pbl.nl/tridion/en/themasites/edgar/emission_data/edgar2-1990). For oceanic emissions, the monthly varying emissions provided by Bouwman et al. (1995) (mostly based on Nevison et al., 1995) and Jin and Gruber (2003) were combined, but scaled by 0.45 and 0.55, respectively. For anthropogenic emissions, we used the annual mean emissions from EDGARv4.2 (covering 1970–2000; <http://edgar.jrc.ec.europa.eu>) for 1984–1999, and from EDGARv4.2 FT2010 (covering 2000–2010) for 2000–2010, but the emissions from EDGARv4.2 were scaled so that the global total emissions of each source category were consistent in 2000 between EDGARv4.2 and EDGARv4.2 FT2010. The anthropogenic emissions for 2011 were kept the same as those in 2010. For emissions from biomass burning, we used the monthly varying

19959

emissions from the REanalysis of the TROpospheric chemical composition over the past 40 years (RETRO, covering 1960–2000; Schultz et al., 2008) for the period 1984–1996, and from the Global Fire Emissions Database (GFED3.1, covering 1997–2011; van der Werf et al., 2010) for 1997–2011, but emissions of RETRO were scaled so that the global total emissions were consistent in 1997 between RETRO and GFED3.1.

This base emission scenario was multiplied by a single scaling factor that was homogeneous in space and time, and used for the simulations of each N_2O isotopocule. The model was optimized for both the long-term trends and north-to-south gradients of tropospheric N_2O isotopocules using the observed data. For the long-term trend optimization, we prepared small and large emission scenarios for each isotopocule by scaling as mentioned above. The scaling factors and mean annual total emissions for the period 1991–2001 are shown in Table 2, and temporal changes in the emissions are shown in Fig. S1 in the Supplement. To optimize the north-to-south gradients, we additionally scaled the emissions using different factors for both hemispheres, but evenly within each hemisphere. The scaling factors were selected so that the average ratio of Northern Hemispheric emissions (E_{NH}) to Southern Hemispheric emissions (E_{SH}) for the period 1991–2001 became 0.8 and 1.3 times the ratio of the base emission scenario for small and large $E_{\text{NH}} : E_{\text{SH}}$ ratio cases, respectively. By this operation, the $E_{\text{NH}} : E_{\text{SH}}$ ratio of the base emission scenario of about 1.5 became about 1.2 and 2.0 for the small and large emissions scenarios, respectively. The horizontal and latitudinal distributions of these emissions are shown in Fig. S1. We regard this range (1.2–2.0) as sufficient, based on our model's hemispheric transport feature in previous N_2O modelling studies, in which the ACTM could well reproduce the north-to-south gradients of the atmospheric N_2O mole fraction with the range of the $E_{\text{NH}} : E_{\text{SH}}$ ratio from 1.3 to 1.9 (Ishijima et al., 2010; Thompson et al., 2014b, c). Finally, we prepared four different emission scenarios for each N_2O isotopocule: small and large global total emissions, and small and large $E_{\text{NH}} : E_{\text{SH}}$ ratios.

19960

the initial ranges for searching the optimal f values were set to a relatively wide range of -1 to 2 . The optimal f values were searched by sequentially changing the values, the intervals and ranges being gradually reduced. In the actual calculation, the first guess of the combination ($f_{E,1}$ and $f_{I,1}$) was obtained with an accuracy of 0.3 in the range of -1 to 2 , the second guess ($f_{E,2}$ and $f_{I,2}$) with an accuracy of 0.15 in the ranges of $f_{E,1} \pm 0.75$ and $f_{I,1} \pm 0.75$, the third guess ($f_{E,3}$ and $f_{I,3}$) with an accuracy of 0.075 in the ranges of $f_{E,2} \pm 0.375$ and $f_{I,2} \pm 0.375$, and the final results were obtained with an accuracy better than 10^{-10} . All results for the f values eventually became between 0 and 1 . The uncertainty caused by the optimization method was estimated using a Monte Carlo approach for the f values, by assigning random errors to the observational data 100 000 times. The random errors were taken from a Gaussian distribution representing the measurement standard error. Uncertainty in the surface emissions was also simultaneously estimated using Eq. (11c). Further details of this optimization procedure are provided in the Supplement.

4.2.2 Model optimization for tropospheric north-to-south gradient and the Northern Hemisphere to Southern Hemisphere emission ratio

The Northern Hemisphere to Southern Hemisphere emission ratio (e) was optimized in almost the same manner as the long-term trend, but more simply (Fig. 2). Time series data, reconstructed from analysis of firn air samples obtained from polar ice sheets (Table 1; Sect. 3.2) were used for this. As shown in Fig. 2, this optimization was performed after the model had been optimized for the long-term trend, because the emission ratio optimization has greater freedom with respect to the f values because of the use of only the inter-pole difference (not the absolute value) and the relatively large measurement error compared to the signal. As described in Sect. 4.1.3, we prepared two different emission scenarios with small and large emission ratios for each isotopocule, and optimized e as follows:

19965

$$S(e_{\text{opt}}) = f_e S(e_S) + (1 - f_e) S(e_L), \quad (14a)$$

$$e_{\text{opt}} = f_e e_S + (1 - f_e) e_L, \quad (14b)$$

where e_S , e_L , and e_{opt} are emission scenarios with small, large, and optimized emission ratios, respectively. As constrained by the observation data, the interhemispheric differences rather than the raw values of the time series from the firn air analysis were used. The time series was fitted using a spline curve and averaged over the period 1991–1998, and then the value of NGR, after subtracting the mean of the values of DFJ and H72, was used for optimization, because model values in the Southern Hemisphere are already optimized to fit the NMY data, and its standard scales differ from those for the firn data. The corresponding values are shown in Table 3. More details of this optimization are described in the Supplement.

There is no site preference information ($\delta^{15}\text{N}^\alpha$ and $\delta^{15}\text{N}^\beta$, or $\delta^{15}\text{N}^{\text{sp}}$) available from the firn data of Ishijima et al. (2007), and no data on the interhemispheric difference of site preference have been published to date. To optimize the north–south gradients by our method, we need to assume a certain value for the $\delta^{15}\text{N}^{\text{sp}}$ gradient. Therefore, we set the value and its uncertainty so that the estimated $\delta^{15}\text{N}^{\text{sp}}$ value and its uncertainty range for each hemisphere's total sources did not exceed the range of the $\delta^{15}\text{N}^{\text{sp}}$ values for various sources quoted in previous studies (see Fig. 9 in Toyoda et al., 2015). Following sensitivity tests, we concluded that no inter-pole difference of $\delta^{15}\text{N}^{\text{sp}}$ was the most reasonable choice (Table 3), which is the same as that assumed in Toyoda et al. (2013). However, as this value is set just for the optimization calculation, we will not discuss hemispheric $\delta^{15}\text{N}^{\text{sp}}$ values any further in this study.

4.2.3 Tuning of photolytic fractionation

Based on some preliminary test simulations, which indicated that the initial photolytic fractionation values given to the model were slightly underestimated, we decided to simply tune the photolytic fractionation in the model. This was achieved by comparing

19966

ε s derived from Rayleigh plots of observation and model results in the stratosphere. As described above, the model was first optimized for long-term trends and north-south gradients in the troposphere, but actually the optimizations were completed for two independent model simulations, in which only photolytic fractionation was different. Then, the best fit to observed ε s were obtained by interpolating the two simulation results.

The ε is often used as one of the indices for diagnosing the degree of isotopocule fractionation caused by photochemical reactions in the stratosphere (e.g., Toyoda et al., 2004; Kaiser et al., 2006). In this study, it was defined as the slope of linear fitting to the Rayleigh plot of the isotopocule data, following the definition by Toyoda et al. (2004; referred to as “isotopomer enrichment factors” therein). In the Rayleigh plot, $\ln\{(\delta + 1)/(\delta_0 + 1)\}$ is plotted against $\ln\{[N_2O]/[N_2O]_0\}$. Here, δ and $[N_2O]$ are the relative isotopocule ratio difference and N_2O mole fraction, respectively, and those without and with the subscript 0 indicate the values in the stratosphere and of the origin, respectively. The origin ($[N_2O]_0$) is tropospheric N_2O , which has not yet suffered from photochemical loss. The air mass in the stratosphere is older than that in the troposphere, because it takes time for the tropospheric air to reach the middle to upper part of the stratosphere. The age of the air in the stratosphere is known to range from near zero to more than five years, depending on the altitude, latitude, and season; in the case of the air at the surface this was set to an age of zero years. Therefore, the N_2O mole fraction and isotopocule ratios of the origin for the air in the stratosphere are supposed to be those of the air in the troposphere in the past. In this study, we used the age of air calculated in the model to determine the values for the original air in the troposphere in the past. The N_2O mole fraction and isotopocule ratios observed at NMY, extrapolated back in time by linear fit, were used as the origin values. Actually, it is difficult to precisely determine the past values, as there are no high-precision measurement data available before 1990, but we regard the error of around 1% in the ε s as acceptable for these calculations, considering the large vertical gradients in the stratosphere. In addition, as discussed by Ishijima et al. (2010), the ACTM tends to un-

19967

derestimate the age in the stratosphere. However, even if the age differs by a maximum of two years between model and observation, the ε value does not change significantly, as temporal changes in the N_2O mole fraction and isotopocule ratios in the troposphere are quite small compared with the vertical gradients in the stratosphere.

The underestimation of the ε in the model might come from underestimation of the isotopocule fractionation caused by reaction with $O(^1D)$ in the model. However, the absolute value of the experimentally determined fractionation constant for photolysis (von Hessberg et al., 2004) are larger by about one order of magnitude compared to those for the $O(^1D)$ reaction (Kaiser et al., 2002). Overestimation of N_2O loss by the $O(^1D)$ reaction may lead to underestimation of the fractionation in the stratosphere by relative increase of the reaction with small isotopic fractionation. Lastly, excessive mixing and transport rates may also cause the apparent stratospheric fractionation to be too small (Kaiser et al., 2006).

We considered that the actual cause for the deficiencies of the stratospheric model simulations was not so important in this study focusing on the tropospheric N_2O , as long as vertical profiles of N_2O mole fraction and isotopocule ratios and apparent isotopic fractionation ε in the stratosphere were realistic. Therefore, we “corrected” the stratospheric model by artificially enhancing the photolysis isotope fractionation. To cover the range of observed ε values by model, photolysis rates of $^{14}N^{15}N^{16}O$, $^{15}N^{14}N^{16}O$, and $^{14}N^{14}N^{18}O$ were scaled by a factor of 0.985 (1.5% reduced photolysis for the heavy isotopocules, leading to larger fractionation). This scaling leads to an increase of the fractionation constants by about 14%, outside the uncertainty of the experimental results of von Hessberg et al. (2004; Figs. 3a, b and 4a, b) of about 2% (1σ) in the stratospherically relevant wavelength range.

Another motivation for adjusting the photolysis rates in the model, as described in Sect. 4.1.1, was that the wavelength resolution of the photolysis calculation in the ACTM was coarse, being only parameterized below 200 nm by a simple scheme, and separated into only three bins above 200 nm, whereas the photolysis of ozone, which is important for the production of $O(^1D)$ in the stratosphere, was calculated in nine wave-

19968

length bins. The coarse wavelength resolution could lead to the uncertainty of N_2O isotopocule fractionations calculated in the ACTM, and the adjustment should take this into account.

The mean ε for all balloon and aircraft observations in the stratosphere (Toyoda et al., 2004; Kaiser et al., 2006), which is the slope of the linear fit to the Rayleigh plots, was used to tune the photolytic fractionation (Fig. 4). The ε s calculated from two simulations with the original and 1.5% reduced photolysis rates, which were already optimized for tropospheric values (Sect. 4.2.1 and 4.2.2), were combined to produce the observed ε s as follows:

$$\varepsilon_{\text{obs}} \approx \varepsilon_{\text{tun}} = f_{\varepsilon} \varepsilon_{\text{org}} + (1 - f_{\varepsilon}) \varepsilon_{\text{red}}, \quad (15a)$$

$$J_{\text{tun}} = f_{\varepsilon} J_{\text{org}} + (1 - f_{\varepsilon}) J_{\text{red}} = (0.015 f_{\varepsilon} + 0.985) J_{\text{org}}, \quad (15b)$$

where J is the photolysis rate, and the subscripts tun, org, and red indicate tuned, simulated using the original photolysis rate (based on von Hessberg et al., 2004), and 1.5% reduced photolysis rate ($J_{\text{red}} = 0.985 J_{\text{org}}$), respectively. We used the 1.5% reduced photolysis rates only in simulations of $^{14}\text{N}^{15}\text{N}^{16}\text{O}$, $^{15}\text{N}^{14}\text{N}^{16}\text{O}$, and $^{14}\text{N}^{14}\text{N}^{18}\text{O}$, so f_{ε} for $^{14}\text{N}^{14}\text{N}^{16}\text{O}$ was always 1. The values of f_{ε} for the heavier isotopocules were calculated by assigning the slope values shown in Fig. 4 to Eq. (15a). The results are shown in Table S1. This approach to tuning the photolytic fractionations is an approximation, as Fig. 4 shows that data scatter in the Rayleigh plots and the slopes (ε s) changing with $\ln\{[\text{N}_2\text{O}]/[\text{N}_2\text{O}]_0\}$ or altitude, as discussed in Toyoda et al. (2004) and Kaiser et al. (2006). However, we regard this relatively rough tuning approach as sufficient, considering that the main purpose of this study is to reproduce long-term trends of tropospheric N_2O isotopocules and to characterize isotopic signatures of global and hemispheric total sources. We discuss the impact of the photolytic fractionation on the source estimates later.

19969

5 Results and discussion

5.1 Temporal variations at Neumayer station

Figure 5 shows the time series of N_2O mole fraction and $\delta^{15}\text{N}^{\text{bulk}}$, $\delta^{18}\text{O}$, $\delta^{15}\text{N}^{\alpha}$, $\delta^{15}\text{N}^{\beta}$, and $\delta^{15}\text{N}^{\text{sp}}$ at NMY, Antarctica, derived from both observations (Röckmann and Levin, 2005) and the optimized model. Standard scales for the observational data are described in Sect. 3.2. The ACTM reproduces the observed results reasonably well overall, showing standard errors of the observational data around the optimized model data (N_2O : $0.1 \text{ nmol mol}^{-1}$, $\delta^{15}\text{N}^{\text{bulk}}$: 0.005 ‰ , $\delta^{18}\text{O}$: 0.005 ‰ , $\delta^{15}\text{N}^{\alpha}$: 0.03 ‰ , $\delta^{15}\text{N}^{\beta}$: 0.03 ‰ , $\delta^{15}\text{N}^{\text{sp}}$: 0.05 ‰) comparable to or better than those of the measurements (shown by error bars in Fig. 5). The results indicate that the model optimization was successful. In addition, it is also evident that the agreement between the model and the observations is much better for mole fraction, $\delta^{15}\text{N}^{\text{bulk}}$, and $\delta^{18}\text{O}$ than for $\delta^{15}\text{N}^{\alpha}$, $\delta^{15}\text{N}^{\beta}$, and $\delta^{15}\text{N}^{\text{sp}}$, as the former components are almost overlapping within the error ranges of the model and observations, whereas the latter components often deviate far from the error ranges. Röckmann and Levin (2005) attributed this data scatter to analytical causes, which make $\delta^{15}\text{N}^{\alpha}$ and $\delta^{15}\text{N}^{\beta}$ deviate in opposite directions and further enhances $\delta^{15}\text{N}^{\text{sp}}$ deviation from the model results. This is probably a reasonable explanation, considering that the variability of $\delta^{15}\text{N}^{\text{bulk}}$ and $\delta^{18}\text{O}$ are reasonably simulated by the model despite there being no spatiotemporal variations in the isotopocule ratios of the surface sources given in the model. Meanwhile, Toyoda et al. (2015) showed that $\delta^{15}\text{N}^{\text{bulk}}$ and $\delta^{18}\text{O}$ vary in similar directions depending on various source types, whereas $\delta^{15}\text{N}^{\text{sp}}$ shows a different tendency from them. Certainly, we cannot exclude the possibility that such features of the site preference data cause more scatter in the atmosphere because of some source-related influence, as Park et al. (2012) raised the possibility that biomass burning was the cause of increased variability in $\delta^{15}\text{N}^{\alpha}$ during the El Niño years of 1997–1998. However, in this study we focus on the long-term trends rather than such short-term variations.

19970

The model significantly underestimates the vertical gradients of N_2O mole fraction by about 20% and isotopocule ratios by about 60% over Kiruna. During the balloon observations, almost all air samplings were conducted within the polar vortex. The vortex prevents the air outside the vortex, with a higher N_2O mole fraction and lower isotopocule ratios, from being transported into the vortex, thus creating a large gradient across the vortex region sometimes exceeding $100 \text{ nmol mol}^{-1}$ in mole fraction around 25 km altitude (Greenblatt et al., 2002). Also, the thermal exchange is disturbed, so the upper altitude air, which has a lower N_2O mole fraction and higher isotopocule ratios, is downwelling due to the strong radiative cooling, thereby contributing to the gradient across the vortex. The ACTM tends to simulate a weaker polar vortex than is actually the case. This feature has already been discussed by Ishijima et al. (2010), who compared ACTM results with the Aura Microwave Limb Sounder (Aura-MLS) satellite N_2O mole fraction data, and showed that the ACTM overestimated the stratospheric mole fraction in the polar vortex in the winter hemisphere. Therefore, this model transport deficiency probably causes the overestimation of the N_2O mole fraction and underestimation of the isotopocule ratios over Kiruna. In the polar vortex, chemical losses of N_2O are very weak due to less sunlight, so variations of N_2O isotopocules in the vortex are mostly determined by transport of the air-mass outside the vortex. It means that ϵ_s in the vortex strongly reflect those outside the vortex. In fact, ϵ_s over Kiruna (Fig. S3) show good agreement between the observations and the model, indicating that the chemistry is reasonable but that the transport makes the profiles unrealistic.

We also need to consider the possibility that the overestimation of mole fraction and underestimation of isotopocule ratios in the polar vortex affect the tropospheric N_2O through STE. However, we do not regard this aspect of the ACTM as too serious with respect to reproducing long-term trends of N_2O isotopocules in the troposphere and estimating the isotopic signatures of the surface sources. Our optimized model shows the troposphere–stratosphere N_2O flux of $66 \text{ Tg a}^{-1} \text{ N}$ and the stratosphere–troposphere N_2O flux of $54 \text{ Tg a}^{-1} \text{ N}$ (calculated using values in Table S3), which are quite similar to those calculated in Toyoda et al. (2013). Considering that the ratio of

19973

N_2O mass in the polar region to that in mid-high latitudes, where the stratosphere–troposphere fluxes occur, is about 10%, the fluxes for the period of the strong polar vortex is $3 \text{ Tg a}^{-1} \text{ N}$, assuming the fluxes contribute to the annual fluxes by 50%. Considering pressure weighted mean differences of the mole fraction and $\delta^{15}\text{N}^{\text{bulk}}$ in the altitude range of 10–15 km, which is important for the STE, are about 20 nmol mol^{-1} and -1 ‰ ([model] – [observation]), respectively (Fig. 6), the model is supposed to underestimate the iso-flux from the stratosphere to the troposphere in the polar region by about $2 \text{ Tg a}^{-1} \text{ N ‰}$. It can be translated into about 0.1% overestimation of $\delta^{15}\text{N}^{\text{bulk}}$ in the final isotopic estimate of the global total sources in this study (Table 4). Here, the relative contribution of the polar region to the stratosphere–troposphere fluxes is uncertain, but trebling the contributing ratio leads to 0.4% overestimation of $\delta^{15}\text{N}^{\text{bulk}}$ in the isotopic estimate of the global total sources. It is obviously the maximum case, so it is thought that the uncertainty in the final source estimation due to the model deficiency for simulating the vertical profiles in the polar vortex is smaller than that due to the measurement. There is also the possibility that seasonal variations of the N_2O isotopic compositions in the troposphere are weakened in the model due to the underestimation of the vertical profiles in the polar stratosphere. However, we need more specific modelling and analysis to discuss the issue, which is also beyond the scope of this study.

In terms of the global budget of N_2O , the vertical profiles in the tropical and mid-latitude stratosphere are more important. N_2O enters the stratosphere in the tropics by convective uplift, and is then transported to higher altitudes/latitudes mainly by the Brewer–Dobson circulation. In this way, N_2O is decomposed by photochemical reactions, and suffers from kinetic isotopic fractionation. As a result, the N_2O mole fraction decreases and isotopocule ratios increase at higher altitudes/latitudes (Fig. S4). This latitudinal and vertical structures of the N_2O mole fraction and isotopocule ratios are reasonably reproduced by the model, except over Kiruna (Figs. 6 and S2). Over Hyderabad, India, the vertical gradients are small, because N_2O is not as exposed to photochemical losses just after entering the stratosphere across the tropopause at around

19974

are the standard errors of the measurement data around the long-term trend derived by a spline fitting curve to the data (Ishijima et al., 2007; the Supplement).

Table 3 indicates that the interhemispheric gradients of atmospheric N₂O mole fraction and isotopocule ratios in the optimized model are slightly smaller than the observed 5
interpolar gradients. We attribute this to the latitudinal gradients as well as the vertical gradients within the hemisphere (Fig. 8), because the firn air samples were collected from stations at high elevations in high latitudes, such as NGR at 75° N/2959 m a.s.l., and DFJ at 77° S/3810 m a.s.l. (Table 1), and there are some gradients from the equator to the poles, especially significantly in the Southern Hemisphere (Fig. 7). Figure 8
10 shows that the ACTM realistically simulates these latitudinal and vertical distributions, which are produced by isotopically lighter N₂O emitted from surface sources and isotopically heavier N₂O mixed-in from the stratosphere. The vertical gradients in the troposphere are actually very small, showing the maximum gradients, between the surface and 8 km altitude, of about 1.3 nmol mol⁻¹, 0.07 and 0.06 ‰ for mole fraction, 15
 $\delta^{15}\text{N}^{\text{bulk}}$, and $\delta^{18}\text{O}$, respectively, in the polar regions, and even small being almost zero in the tropics, where convective transport is quickly bringing near surface N₂O to the upper troposphere and further into the stratosphere. Magnitudes of the vertical gradients are comparable to those of the interhemispheric gradients (Table 3), and important for hemispheric source estimates using the atmospheric observational data from high
20 elevation firn stations in the polar regions. As the model data at the locations of the firn stations were used for our model optimization, we expect that the 3-D model-based estimates of the isotopic signature of the sources could differ from the estimates made using a two-box model, in which the interhemispheric differences are directly derived from the firn measurement data (Toyoda et al., 2013). This would be important if we
25 wished to translate the atmospheric observation data into the surface source information as precisely as possible, as is the case in inverse modelling (Hirsch et al., 2006; Huang et al., 2008; Thompson et al., 2014c).

Optimization of the atmospheric values was achieved by adjusting the global and hemispheric total emissions of four N₂O isotopocules. As explained in Sect. 4.1.3,

19977

the optimization modifies the hemispheric total emissions but does not modify the emission distributions within the hemisphere; as a result, the isotopocule ratios from the sources become homogeneous in each hemisphere (Fig. 7). $\delta^{15}\text{N}^{\text{bulk}}$ of the total
5 sources shows reasonable results of 10 ‰ lower in the Northern Hemisphere than in the Southern Hemisphere because there are more land sources with relatively lower $\delta^{15}\text{N}^{\text{bulk}}$ (Toyoda et al., 2015) in the Northern Hemisphere, while the area of the ocean with relatively higher $\delta^{15}\text{N}^{\text{bulk}}$ is larger in the Southern Hemisphere. Interestingly, despite almost the same $\delta^{18}\text{O}$ levels in both hemispheric total sources, the $\delta^{18}\text{O}$ of the atmospheric N₂O is lower in the Northern Hemisphere. This can be simply explained
10 by the dilution of isotopically heavier tropospheric N₂O by lighter N₂O emitted from surface sources when Northern Hemispheric emissions are larger, given even isotopocule fractionation caused by the stratospheric chemical loss in both hemispheres. In fact, the interhemispheric transport smoothes out the north–south gradient to some extent, but the tendency would not change. The $\delta^{15}\text{N}^{\text{sp}}$ shows completely the opposite tendency, the same atmospheric $\delta^{15}\text{N}^{\text{sp}}$ values in both hemispheres (assumed only for the optimization, see Sect. 4.2.2), but the source $\delta^{15}\text{N}^{\text{sp}}$ is higher in the Northern Hemisphere. The logic is exactly the same as that for $\delta^{18}\text{O}$, but in this case the extra $\delta^{15}\text{N}^{\text{sp}}$ input from the surface sources increases the atmospheric value in the Northern Hemisphere.
15 We note that the north–south gradients in the atmosphere, as well as the emissions and isotopic signatures of surface sources, are highly dependent on the transport features of the model, such as interhemispheric transport, convection, and STE, as well as the emission distribution used in the model. On these points, the ACTM shows the best result of north–south gradient for the atmospheric N₂O mole fraction in comparison with other models (Thompson et al., 2014b, c); therefore, the N₂O isotopocule ratios are also expected to be reliable, both in the atmosphere and for top-down source
25 estimates.

19978

(Toyoda et al., 2015). The interhemispheric difference in $\delta^{15}\text{N}^{\text{bulk}}$ estimated by Toyoda et al. (2013; about 4‰) is slightly smaller than ours (about 10‰). This can be attributed to differences in several factors, such as latitudinal and vertical transports (interhemispheric and stratosphere–troposphere exchanges) and distributions (interhemispheric and vertical gradient), which are explicitly simulated in the ACTM but assumed in the two-box model of Toyoda et al. (2013). The latitudinal emission distribution in our model (Fig. 7) also has a significant influence on these hemispheric-scale estimates based on the atmospheric observation data, as discussed in Sect. 5.3. Tendencies for our bottom-up estimates, in which both $\delta^{15}\text{N}^{\text{bulk}}$ and $\delta^{18}\text{O}$ of the total sources are higher in the Southern Hemisphere than in the Northern Hemisphere, are similar to those of Toyoda et al. (2013). As expected, the results directly reflect the fractions of isotopically lighter natural and anthropogenic soil emissions, and of isotopically heavier oceanic emissions, in each hemisphere; more land and less ocean in the Northern Hemisphere, and less land and more ocean in the Southern Hemisphere make the total sources isotopically lighter and heavier, respectively.

We also examined the sensitivities of the emissions and isotopocule ratios of the hemispheric total sources to interhemispheric differences in the atmospheric N_2O mole fraction and isotopocule ratios in our top-down estimates. In these experiments, we assumed interhemispheric differences in the atmospheric N_2O mole fraction and/or isotopocule ratios to be more or less than the real by 50% by changing the values observed (Table 3), and then optimized the Northern Hemisphere to Southern Hemisphere emission ratio in the model (Sect. 4.2.2; Fig. 2) to reproduce the assumed interhemispheric differences in the atmosphere. Figure 9 (top) indicates that even when emissions in both hemispheres are the same, the mole fraction is higher by about 0.6 nmol mol^{-1} in the Northern Hemisphere. This is mainly caused by the latitudinal emission distribution used in the model, in which more emissions are located at higher latitudes in the Northern Hemisphere (Fig. S1c). For example, as an extreme case, if the same amount of N_2O is emitted only at the North Pole and in the tropics of the Southern Hemisphere over a period of time, the N_2O mole fraction would always be

19981

higher in the Northern Hemisphere, because it takes several months for N_2O in the Arctic to reach the equator while N_2O emitted in the tropics quickly diffuses into both hemispheres and partly into the stratosphere. These latitudinal and vertical transportations of the emitted N_2O are also highly model-dependent (Denning et al., 1999). Similar to the above case, the atmospheric N_2O isotopocule ratios are lower in the Northern Hemisphere than in the Southern Hemisphere, even when there is no interhemispheric difference in the N_2O emissions (corresponding to zero on the y axis in Fig. 9, top, and to the sensitivity line between the thick solid and dashed lines in Fig. 9, bottom) and in the isotopocule ratios of the total sources (corresponding to zero on the y axis in Fig. 9, bottom). The features are also thought to originate from latitudinal emission distribution in our model (Fig. 7). As expected, the sensitivity of the atmospheric gradient to changes in the hemispheric source values is almost the same for $\delta^{15}\text{N}^{\text{bulk}}$ and $\delta^{18}\text{O}$, but also for $\delta^{15}\text{N}^{\text{sp}}$, with the slopes of all lines being similar ($240 \pm 10\text{‰‰}^{-1}$ in Fig. 9, bottom). These results indicate that the interhemispheric gradient of the N_2O isotopocule ratio is determined almost completely by the emissions in both hemispheres and interhemispheric transport, and much less so by the influence of stratospheric chemistry, which could alter $\delta^{15}\text{N}^{\text{bulk}}$, $\delta^{18}\text{O}$, and $\delta^{15}\text{N}^{\text{sp}}$ in each direction by each kinetic fractionation after emitted from surface sources into the atmosphere.

5.5 Time series of atmospheric N_2O isotopocule ratios at other stations

Figure 10 shows the atmospheric N_2O mole fraction and isotopocule ratios obtained from ground-based observations, firn air analysis, and the optimized model. The trends in the observed mole fraction are reasonably simulated for all stations, but some biases between observations and between observations and model are evident. In the 20th century, the firn data from DFJ and H72 tend to be lower than the observations and model results at NMY. This is likely due to the difference in the standard scales used for the measurements at each station, as the long-term trend is optimized only to the NMY data for the period 1990–2002. After 2000, the model seems to under-

19982

the law of propagation of error) to estimate the isotopocule ratios of hemispheric total sources with an accuracy of 10‰. In addition, for example, in order to estimate monthly emissions of the N₂O isotopic compositions at regional scale, improvements especially for measurement frequency and number of the stations as well as the inter-calibration of the standard would be necessary, assuming that the analytical precisions are those for the NMY data. If successful, it would allow us to incorporate more observation data into our model, thereby enabling improved optimization and more advanced inverse estimation of surface source emissions in the near future.

6 Conclusions

We developed an atmospheric N₂O isotopocule model by incorporating isotopocule fractionation caused by photolysis and oxidation by O(¹D), together with surface fluxes of N₂O isotopocules, in a chemistry-coupled atmospheric general circulation model (ACTM). In addition, we developed a method, based on multi-scenario simulations, to optimize the model for long-term trends, north-to-south gradients in the troposphere, and apparent fractionation constants in the stratosphere, by using atmospheric data obtained from ground-based stations, firn air analysis, and balloon and aircraft observations in the stratosphere. This is the first study to simulate atmospheric N₂O isotopocules using a 3-D chemistry transport model with explicitly prescribed surface fluxes, and to optimize the model using atmospheric observation data.

The optimized model reasonably reproduced the atmospheric N₂O mole fraction and isotopocule ratios observed at Neumayer station, Antarctica, especially the long-term trends; this indicates that the model optimization was successful. Temporal variability in mole fraction, $\delta^{15}\text{N}^{\text{bulk}}$, and $\delta^{18}\text{O}$, including seasonal and synoptic variations, were also comparable between the observations and the optimized model, whereas the simulated $\delta^{15}\text{N}^{\alpha}$, $\delta^{15}\text{N}^{\beta}$, and $\delta^{15}\text{N}^{\text{sp}}$ were much more stable than the highly scattered observations. The model showed regular seasonal cycles for all components, which are produced by seasonality in oceanic emissions and by atmospheric transport, re-

19985

producing observations in mole fraction and $\delta^{15}\text{N}^{\text{bulk}}$ relatively well, but the cycles were not as clear in the other observed isotopic components.

The model reproduced the vertical profiles of N₂O mole fraction and isotopocule ratios in the stratosphere reasonably well, which decrease and increase with increasing altitude, respectively. Tuning of photolytic fractionation, using apparent fractionation constants (ϵ_s), improved the model results by slightly increasing the vertical gradients of the isotopocule ratios. However, in the polar vortex, the model significantly underestimated the vertical gradients of both mole fraction and isotopocule ratios by about 20 and 60 %, respectively. This was caused by excess transport of air with high N₂O mole fraction and low isotopocule ratios from lower latitudes into the vortex, as the model has insufficient dynamic isolation.

Optimization of the north–south gradient was successfully done. The mean latitudinal gradient of atmospheric N₂O mole fraction for the period 1991–2001 in the optimized model was consistent with that of independent observational data from GAGE/AGAGE within the uncertainty range. Although there are no independent data available with which to validate latitudinal gradients of optimized isotopocule ratios, we found that the model could reasonably simulate the vertical and latitudinal gradients within the hemispheres. The fact that the respective interhemispheric differences of 1 nmol mol⁻¹, 0.1 and 0.04‰ for mole fraction, $\delta^{15}\text{N}^{\text{bulk}}$ and $\delta^{18}\text{O}$ were smaller than the respective inter-polar differences of 1.3 nmol mol⁻¹, 0.12 and 0.06‰ was due to the vertical and latitudinal distributions within the hemispheres. The tropospheric vertical gradients between the surface and 8 km altitude were 1.3 nmol mol⁻¹, 0.07 and 0.06‰ for mole fraction, $\delta^{15}\text{N}^{\text{bulk}}$, and $\delta^{18}\text{O}$, respectively, in the polar regions, and are comparable to the interhemispheric gradients. The gradients are very small, but are important for isotopically characterizing surface sources using atmospheric observation data from the locations of the individual stations. Such tropospheric latitudinal and vertical gradients lead to differences in the isotopic characterization of hemispheric total sources when compared with a simple two-box model, which in some cases directly uses station data as the hemispheric representative values. The 3-D structures simulated by the model

19986

- Machida, T., Nakazawa, T., Fujii, Y., Aoki, S., and Watanabe, O.: Increase in the atmospheric nitrous oxide concentration during the last 250 years, *Geophys. Res. Lett.*, 22, 2921–2924, 1995.
- McLinden, C. A., Prather, M. J., and Johnson, M. S.: Global modelling of the isotopic analogues of N₂O: stratospheric distributions, budgets, and the ¹⁷O-¹⁸O mass-independent anomaly, *J. Geophys. Res.*, 108, 4233, doi:10.1029/2002JD002560, 2003.
- Minschwaner, K., Salawitch, R. J., and McElroy, M. B.: Absorption of solar radiation by O₂: implications for O₃ and lifetimes of N₂O, CFC₁₃, and CF₂Cl₂, *J. Geophys. Res.*, 98, 10543–10561, 1993.
- Mohn, J., Wolf, B., Toyoda, S., Lin, C.-T., Liang, M.-C., Brüggemann, N., Wissel, H., Steiker, A. E., Dyckmans, J., Szewc, L., Ostrom, N. E., Casciotti, K. L., Forbes, M., Giesemann, A., Well, R., Doucet, R. R., Yarnes, C. T., Ridley, A. R., Kaiser, J., and Yoshida, N.: Inter-laboratory assessment of nitrous oxide isotopomer analysis by isotope ratio mass spectrometry and laser spectroscopy: current status and perspectives, *Rapid Commun. Mass Sp.*, 28, 1995–2007, doi:10.1002/rcm.6982, 2014.
- Morgan, C. G., Allen, M., Liang, M. C., Shia, R. L., Blake, G. A., and Yung, Y. L.: Isotopic fractionation of nitrous oxide in the stratosphere: comparison between model and observations, *J. Geophys. Res.-Atmos.*, 109, D04305, doi:10.1029/2003JD003402, 2004.
- Nakazawa, T., Ishizawa, M., Higuchi, K., and Trivett, N. B. A.: Two curve fitting methods applied to CO₂ flask data, *Environmetrics*, 8, 197–218, 1997.
- Nanbu, S. and Johnson, M. S.: Analysis of the ultraviolet absorption cross sections of six isotopically substituted nitrous oxide species using 3D wave packet propagation, *J. Phys. Chem. A*, 108, 8905–8913, doi:10.1021/jp048853r, 2004.
- Nevison, C. D., Weiss, R. F., and Erickson III, D. J.: Global oceanic emissions of nitrous oxide, *J. Geophys. Res.*, 100, 15809–15820, 1995.
- Nevison, C. D., Mahowald, N. M., Weiss, R. F., and Prinn, R. G.: Interannual and seasonal variability in atmospheric N₂O, *Global Biogeochem. Cy.*, 21, GB3017, doi:10.1029/2006GB002755, 2007.
- Numaguti, A., Takahashi, M., Nakajima, T., and Sumi, A.: Development of CCSR/NIES Atmospheric General Circulation Model, CGER's Supercomput. Monogr. Rep., 3, 1–48, Tsukuba, Ibaraki, 1997.
- Onogi, K., Tsutsui, J., Koide, H., Sakamoto, M., Kobayashi, S., Hatsushika, H., Matsumoto, T., Yamazaki, N., Kamahori, H., Takahashi, K., Kadokura, S., Wada, K., Kato, K., Oyama, R.,

19991

- Ose, T., Mannoji, N., and Taira, R.: The JRA-25 reanalysis, *J. Meteorol. Soc. Jpn.*, 85, 369–432, 2007.
- Park, S., Atlas, E. L., and Boering, K. A.: Measurements of N₂O isotopologues in the stratosphere: influence of transport on the apparent enrichment factors and the isotopologue fluxes to the troposphere, *J. Geophys. Res.*, 109, D01305, doi:10.1029/2003JD003731, 2004.
- Park, S., Croteau, P., Boering, K. A., Etheridge, D. M., Ferretti, D., Fraser, P. J., Kim, K.-R., Krummel, P. B., Langenfelds, R. L., van Ommen, T. D., Steele, L. P., and Trudinger, C. M.: Trends and seasonal cycles in the isotopic composition of nitrous oxide since 1940, *Nat. Geosci.*, 5, 261–265, doi:10.1038/ngeo1421, 2012.
- Prinn, R. G., Weiss, R. F., Fraser, P. J., Simmonds, P. G., Cunnold, D. M., Alyea, F. N., O'Doherty, S., Salameh, P., Miller, B. R., Huang, J., Wang, R. H. J., Hartley, D. E., Harth, C., Steele, L. P., Sturrock, G., Midgley, P. M., and McCulloch, A.: A history of chemically and radiatively important gases in air deduced from ALE/GAGE/AGAGE, *J. Geophys. Res.*, 105, 17751–17792, 2000.
- Rahn, T. and Wahlen, M.: A reassessment of the global isotopic budget of atmospheric nitrous oxide, *Global Biogeochem. Cy.*, 14, 537–543, 2000.
- Ravishankara, A. R., Daniel, J. S., Portmann, R. W.: Nitrous Oxide (N₂O): the dominant ozone-depleting substance emitted in the 21st century, *Science*, 326, 5949, 123–125, doi:10.1126/science.1176985, 2009.
- Rigby, M., Manning, A. J., and Prinn, R. G.: The value of high-frequency, high-precision methane isotopologue measurements for source and sink estimation, *J. Geophys. Res.*, 117, D12312, doi:10.1029/2011JD017384, 2012.
- Röckmann, T. and Levin, I.: High-precision determination of the changing isotopic composition of atmospheric N₂O from 1990 to 2002, *J. Geophys. Res.*, 110, D21304, doi:10.1029/2005JD006066, 2005.
- Röckmann, T., Kaiser, J., and Brenninkmeijer, C. A. M.: The isotopic fingerprint of the pre-industrial and the anthropogenic N₂O source, *Atmos. Chem. Phys.*, 3, 315–323, doi:10.5194/acp-3-315-2003, 2003.
- Saikawa, E., Prinn, R. G., Dlugokencky, E., Ishijima, K., Dutton, G. S., Hall, B. D., Langenfelds, R., Tohjima, Y., Machida, T., Manizza, M., Rigby, M., O'Doherty, S., Patra, P. K., Harth, C. M., Weiss, R. F., Krummel, P. B., van der Schoot, M., Fraser, P. J., Steele, L. P., Aoki, S., Nakazawa, T., and Elkins, J. W.: Global and regional emissions estimates for N₂O, *Atmos. Chem. Phys.*, 14, 4617–4641, doi:10.5194/acp-14-4617-2014, 2014.

19992

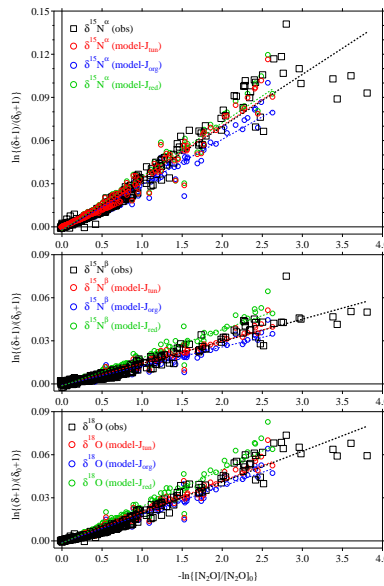


Figure 4. Rayleigh plots for $\delta^{15}\text{N}^\alpha$, $\delta^{15}\text{N}^\beta$, and $\delta^{18}\text{O}$ of stratospheric N_2O from balloon and aircraft observations (obs) and the model results (J_{tun} : with tuned photolysis rate, J_{org} : with original photolysis rate, J_{red} : with 1.5% reduced photolysis rate for heavier isotopocules). Dashed lines represent linear-fits to the Rayleigh plots and the slopes are the apparent fractionation constant (ϵ). The photolysis rate for heavier isotopocules in the model is tuned so that a linear combination of the slopes of the blue and green lines is equivalent to the slope of the black line, $\epsilon_{\text{obs}} (= f\epsilon_{\text{org}} + (1-f)\epsilon_{\text{red}})$. Red line represents model results from the tuned photolysis ($J_{\text{tun}} = fJ_{\text{org}} + (1-f)J_{\text{red}}$).

20003

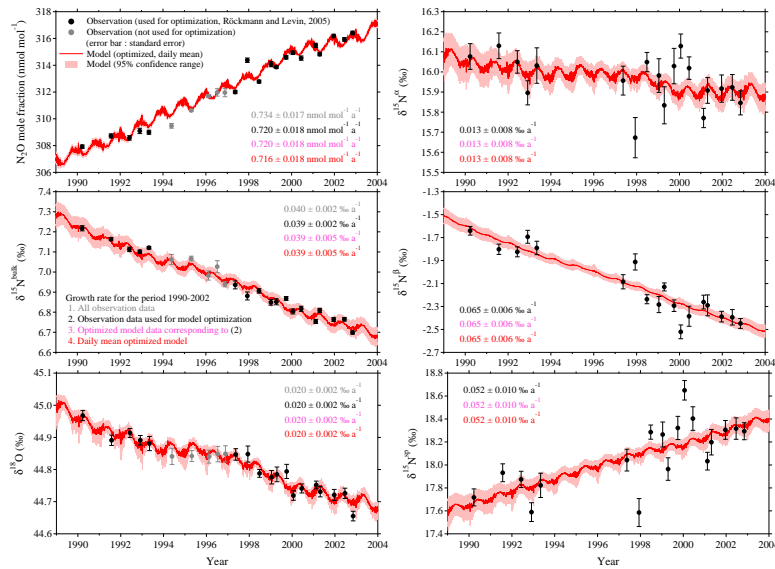


Figure 5. Atmospheric N_2O mole fraction, $\delta^{15}\text{N}^{\text{bulk}}$, $\delta^{18}\text{O}$, $\delta^{15}\text{N}^\alpha$, $\delta^{15}\text{N}^\beta$, and $\delta^{15}\text{N}^{\text{sp}}$ at NMY, Antarctica, observed (Röckmann and Levin, 2005) and simulated by the ACTM.

20004

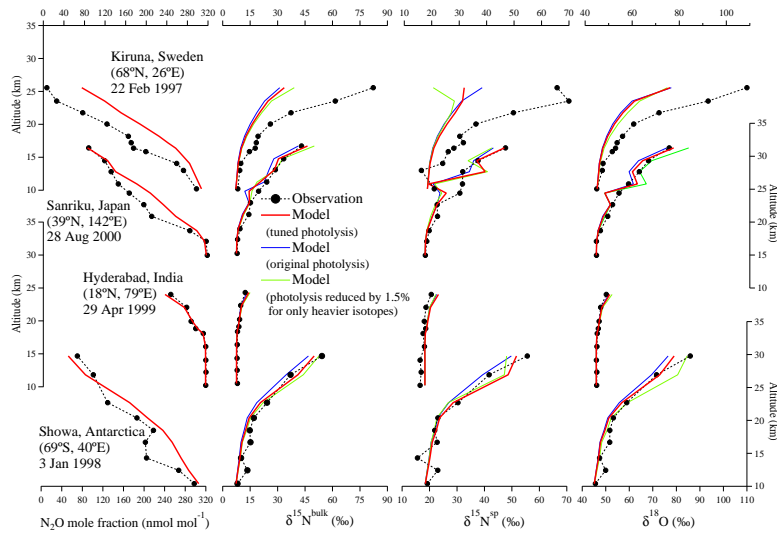
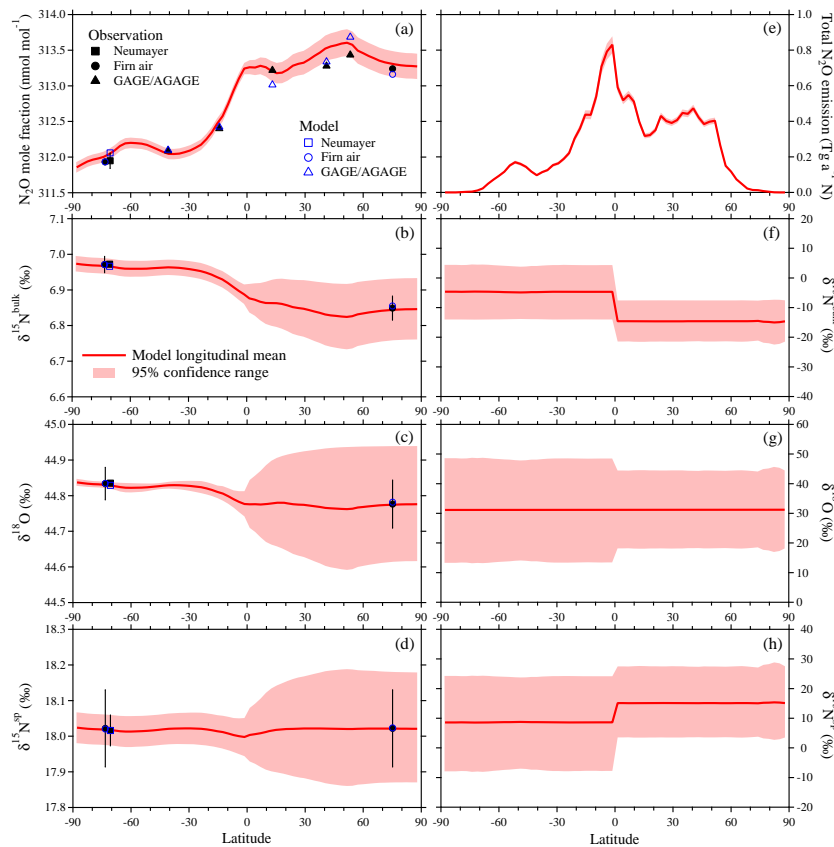


Figure 6. Vertical profiles of N_2O mole fraction, $\delta^{15}\text{N}^{\text{bulk}}$, $\delta^{18}\text{O}$, and $\delta^{15}\text{N}^{\text{sp}}$ in the stratosphere observed using balloon and simulated by the ACTM. For the isotopic results from Hyderabad, as the observed isotopic ratios from Kaiser et al. (2006) were given relative to the tropospheric values, they were rescaled using the simulated values from NMY for the balloon observation day.

20005



20006

Figure 7. Latitudinal distributions of annual means of N_2O , $\delta^{15}\text{N}^{\text{bulk}}$, $\delta^{18}\text{O}$, and $\delta^{15}\text{N}^{\text{sp}}$ in the atmosphere (**a**, **b**, **c** and **d**) and of surface sources (**e**, **f**, **g** and **h**) for the period 1991–2001 from the optimized model, and their 95 % confidence ranges. Annual means of original observation data at NMY and GAGE/AGAGE stations, which are means of the long-term trends derived using a digital-filtering technique (Nakazawa et al., 1997), are plotted, but those at the firn stations, which are means of spline-curves fitted to the data (Ishijima et al., 2007), were adjusted to the means of the optimized model results from DFJ and H72, as the standard scales differ. Error bars for the firn data represent the standard errors of the observation data around the spline-curves. The greater uncertainty in the Northern Hemisphere results from assigning a relatively large uncertainty to the inter-polar difference of the observations in the optimization process, whereas the model is tightly fitted to the NMY data in the Southern Hemisphere.

20007

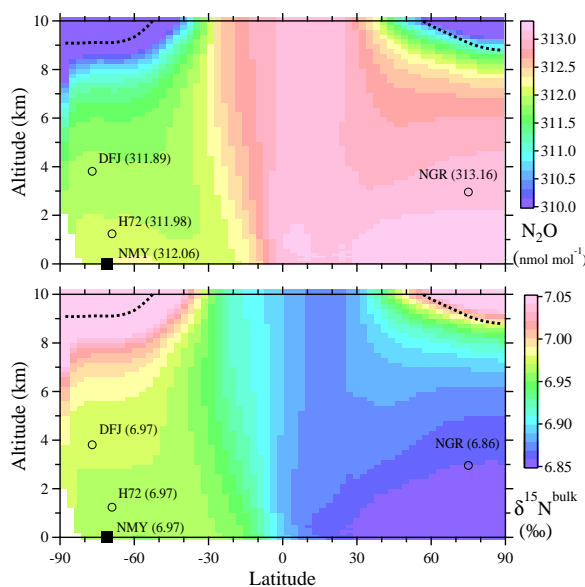


Figure 8. Annual zonal mean atmospheric N_2O mole fraction (top) and $\delta^{15}\text{N}^{\text{bulk}}$ (bottom) in the troposphere for the period 1991–2001 from the optimized model (the daily mean model outputs were simply averaged for the period). Marks represent locations of NMY, NGR, DFJ and H72 (Table 1), and black dotted lines represent tropopause height in the model as defined by a potential vorticity of 3.5 PVU and a potential temperature of 390 K. Values in parentheses represent those simulated for individual stations. $\delta^{18}\text{O}$ and $\delta^{15}\text{N}^{\text{sp}}$ also have almost the same latitudinal and vertical structures as $\delta^{15}\text{N}^{\text{bulk}}$.

20008

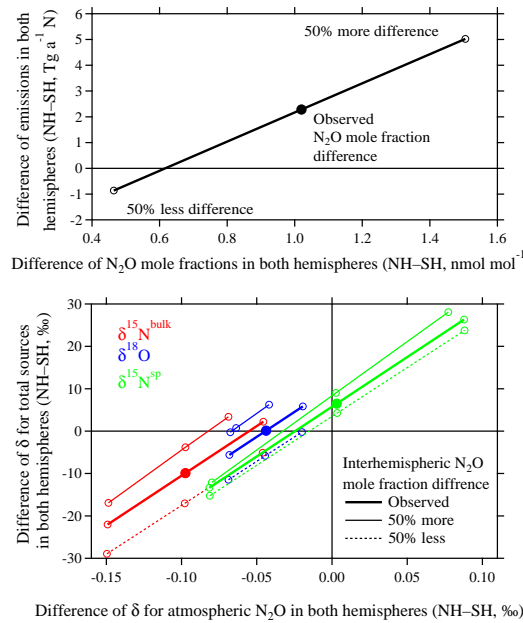
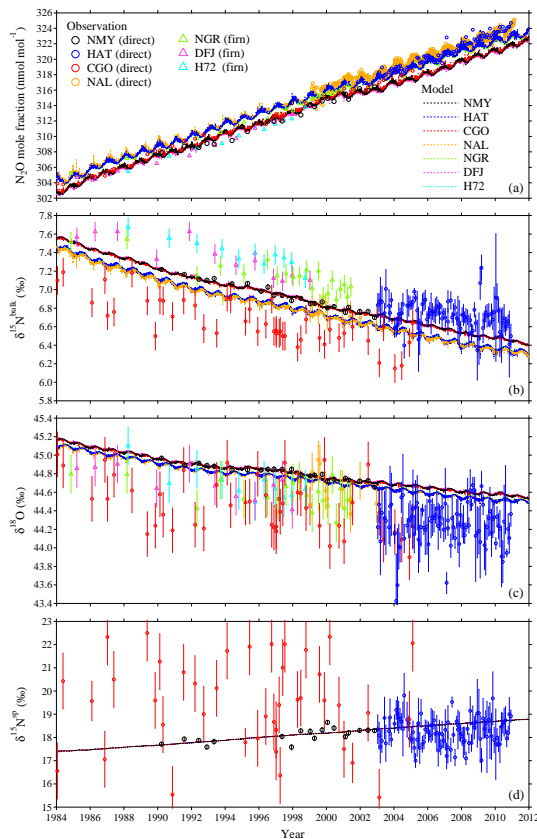


Figure 9. Sensitivities of emissions (top) and $\delta^{15}\text{N}^{\text{bulk}}$, $\delta^{18}\text{O}$, and $\delta^{15}\text{N}^{\text{sp}}$ (bottom) of hemispheric total sources to interhemispheric difference in atmospheric N_2O mole fraction, $\delta^{15}\text{N}^{\text{bulk}}$, $\delta^{18}\text{O}$, and $\delta^{15}\text{N}^{\text{sp}}$ for the period 1991–2001 in the model. The sensitivities were estimated by optimizing the model against the 50% reduced or increased observed interhemispheric difference in atmospheric N_2O mole fraction and isotopic delta values (Table 3), but without changing the data at NMY. Therefore, the estimated global total emissions were similar in all cases ($15.45 \pm 0.03 \text{ Tg a}^{-1} \text{ N}$).

20009



20010

Figure 10. Atmospheric N₂O mole fraction **(a)**, $\delta^{15}\text{N}^{\text{bulk}}$ **(b)**, $\delta^{18}\text{O}$ **(c)**, and $\delta^{15}\text{N}^{\text{sp}}$ **(d)** obtained from ground-based observations, firn air analysis (see Fig. 1 and Table 1 for details of the stations), and the optimized model (daily mean output). The standard scale for each observation was not adjusted and each is plotted at the original scale.